IBRO Neuroscience Reports 18 (2025) 559–573

Contents lists available at ScienceDirect

IBRO Neuroscience Reports

journal homepage: www.sciencedirect.com/journal/IBRO-Neuroscience-Reports

RNF13 variants L311S and L312P associated with developmental epileptic encephalopathy alter dendritic organization in hippocampal neurons

Valérie C. Cabana [a,b,c], Marc P. Lussier [a,b,c,*]

[a] Department of Chemistry, Université du Québec à Montréal, 2101, rue Jeanne-Mance, Montréal, QC H2X 2J6, Canada
[b] CERMO-FC - The Center of Excellence in Research on Ophan Diseases - Fondation Courtois, Université du Québec à Montréal, Montréal, QC H2X 3Y7, Canada
[c] PROTEO - The Quebec Network for Research on Protein Function, Engineering and Applications, Montréal, QC H3C 3P8, Canada

ARTICLE INFO

Keywords:
RNF13
Developmental and epileptic encephalopathy
E3 ubiquitin ligase
Endolysosomal system
Dendrites

ABSTRACT

Developmental and epileptic encephalopathy (DEE) is a group of rare and serious neurological disorders where seizures exacerbate developmental impairment. Recently, genetic mutations in the *RNF13* gene were reported to cause DEE73. Specifically, two leucines from the ubiquitin E3 ligase RNF13 are converted to serine or proline (L311S and L312P). These mutations are located within a dileucine motif, which impairs RNF13's capacity to interact with AP-3. A second motif allows RNF13 to interact with AP-1 when the dileucine sorting motif is altered. The present study demonstrates that RNF13 variants L311S and L312P are trafficked through an AP-1-dependent pathway in HeLa cells. In cultures of primary rat hippocampal neurons, the protein level of the variants is significantly higher in dendrites than for wild-type protein. L311S and L312P variants alter dendritic components similarly to an RNF13 AP-3-defective binding variant or a dominant negative for RNF13's ubiquitin ligase activity. Compared to non-transfected neurons, the variants change the distribution of EEA1-positive early endosomes throughout the dendrites. While the WT alters the distribution of lysosomes (Lamp1-positive) in dendrites, the variants only decrease their presence in proximal dendrites. Unlike the variants, RNF13 WT increases the abundance of PSD-95 in distal dendrites. Interestingly, only the variants with altered dileucine motifs decrease the total number of postsynaptic inhibitory protein Gephyrin puncta. This study reports that genetic variants L311S and L312P mainly act as a dominant negative protein. This research provides valuable insights into the dendritic defects that occur when DEE73-associated genetic variants of RNF13 are present.

1. Introduction

Neurons are highly polarized cells with three main domains (soma, axon, and dendrites) and various subdomains (dendritic spines, axon initial segment and pre- and postsynaptic terminals) (Donato et al., 2019). Each neuron has a single axon exhibiting extensive terminal branches and multiple dendrites with complex arbors extending several centimeters or more (Roney et al., 2022). As protein synthesis and degradation are primarily performed in the soma, efficient bidirectional transport mechanisms and spatial regulation of organelles are crucial to maintain neuron growth, survival and function (Roney et al., 2022; Yap and Winckler, 2022).

Endosomes are essential for maintaining proper neuronal homeostasis by sorting, processing, recycling, storing and degrading internalized molecules or receptors (Huotari and Helenius, 2011). Endolysosomal maturation involves the gradual acidification of endocytic vesicles, leading to the degradation of internalized proteins. This progression is characterized by the transformation of early endosomes into late endosomes and ultimately into lysosomes (Hu et al., 2015). Defects in endolysosomal maturation can lead to various diseases, including, but not limited to, lysosomal storage disorders, neurodegenerative diseases, cancer and infectious diseases (Hu et al., 2015; Tang

Abbreviations: AP, adaptor protein; DEE, developmental and epileptic encephalopathy; DIST, distal; DIV, day in vitro; DN, dominant negative; ECM, extracellular matrix; EEA1, early endosome antigen 1; Endo H, endoglycosidase H; ER, endoplasmic reticulum; GABA, gamma-aminobutyric acid; LL/AA, RNF13 L311A/L312A; Lamp1, lysosomal associated membrane protein 1; MAP2, microtubule-associated protein 2; NT, non-transfected neuron; PNGase F, peptide-N-glycosidase F; PROX, proximal; PSD-95, postsynaptic protein 95; RCAS1, receptor binding cancer antigen expressed in SiSo cells; RNF13, ring finger protein 13; SV, synaptic vesicle; TGN, trans-Golgi network; Ub, ubiquitin.

* Correspondence to: Département de Chimie, Université du Québec à Montréal, Faculté des Sciences, Succ. Centre-ville, Case postale 8888, Montreal, Québec H3C 3P8, Canada.
E-mail address: lussier.marc@uqam.ca (M.P. Lussier).

https://doi.org/10.1016/j.ibneur.2025.04.004
Received 23 December 2024; Received in revised form 19 March 2025; Accepted 4 April 2025
Available online 9 April 2025

et al., 2020; Rebiai et al., 2021; Chao et al., 2023).

Proper targeting to the correct cellular compartment requires packaging cargo proteins into coated vesicles (Sanger et al., 2019). Adaptor protein (AP) complexes play a crucial role in this process as they recognize and concentrate the cargo proteins into vesicular carriers (Dell'Angelica and Bonifacino, 2019). Each AP complex has a specific localization and function (Sanger et al., 2019). Within the endolysosomal system, AP-1 allows bidirectional transport between the trans-Golgi network (TGN) and endosomes, AP-2 is involved in endocytosis and AP-3 regulates trafficking from the TGN and tubular endosomal compartments to late endosomes, lysosomes and lysosome-related organelles (Park and Guo, 2014; Dell'Angelica and Bonifacino, 2019). These AP proteins are heterotetrameric complexes composed of two large subunits (γ/α/δ and β1–3, respectively), one medium-sized subunit (μ1–3) and one small subunit (σ1–3) (Park and Guo, 2014). AP complexes recognize cargo proteins by specific sorting signals on their cytoplasmic tails. The two canonical and well-characterized sorting signals are the tyrosine-based (YxxΦ) and dileucine-based ([D/E]xxxL[L/I]) motifs, where x is any amino acid and Φ is a bulky hydrophobic amino acid (Park and Guo, 2014; Sanger et al., 2019). However, some noncanonical motifs and acidic clusters have also been reported to bind AP-1 and AP-2 (Guo et al., 2013; Navarro Negredo et al., 2017; Cabana et al., 2024). Importantly, AP complexes have specific neuronal functions. AP-1 is responsible for somatodendritic sorting towards postsynaptic terminals, while AP-3 is involved in axonal sorting towards presynaptic terminals and synaptic vesicle (SV) biogenesis (Guardia et al., 2018). Neurological disorders have been linked to genetic mutations in constituent subunits of both AP complexes, demonstrating their importance in neuronal function (Zhang et al., 2024).

Ring Finger Protein 13 (RNF13) is a transmembrane E3 ubiquitin (Ub) ligase localized in the endoplasmic reticulum (ER), Golgi, late endosomes, lysosomes and at the plasma membrane (Cabana and Lussier, 2022). It is suggested to have a role in neurodevelopmental processes. In PC12 cells, the exogenous expression of RNF13 leads to spontaneous neurite growth, while treatment of B35 cells with differentiation-inducing molecule dibutyryl-cAMP doubled RNF13 mRNA expression (Saito et al., 2005; Bocock et al., 2009). Furthermore, RNF13 Ub ligase activity catalyzes ubiquitination of SNARE-associated protein (snapin) to strengthen binding with synaptosome-associated protein 25 (SNAP-25) to regulate the release of neurotransmitters into the synaptic cleft (Zhang et al., 2013). More recently, RNF13 inhibited lysosome maturation through ubiquitination-dependent degradation of lysosomal protein Lamp1 in macrophages following Toll-like receptor (TLR)-triggered response (Liu et al., 2024). While RNF13 is also associated with tumorigenesis, cell migration, invasiveness, cell proliferation, myogenesis and selective autophagy, most molecular mechanisms are yet to be established (Tranque et al., 1996; Zhang et al., 2009; van Dijk et al., 2014; Cheng et al., 2015; Miyakawa et al., 2022; Tan et al., 2022; Lin et al., 2023).

Developmental and epileptic encephalopathy (DEE) are a heterogeneous group of disorders characterized by early-onset epileptic seizures with a developmental impairment that is worsened by epilepsy. While some DEEs result from nongenetic etiologies, an increasing number of genes are reported to cause different DEEs (Guerrini et al., 2023). A recent study reported three unrelated individuals carrying de novo heterozygous mutations within the *RNF13* gene (c.932 T > C, p.L311S; c.935 T > C, p.L312P) causing DEE73 (Edvardson et al., 2019). The phenotype is characterized by epileptic encephalopathy, blindness, congenital microcephaly, failure to thrive and profound developmental delay (Edvardson et al., 2019). We recently analyzed RNF13's sequence and found that the variant proteins L311S and L312P modify a canonical dileucine [D/E]xxxL[L/I] motif, altering their binding to AP-3 and significantly reducing their presence in lysosomes (Cabana et al., 2021). While the RNF13 L311S and L312P proteins variants are encoded by a region of the *RNF13* gene proposed as a hotspot for DEE73 (Taylor et al., 2023), the cellular and molecular mechanisms by which these variants affect neuronal development and lead to a severe childhood neurodevelopmental disease remain unknown. Here, we used primary rat hippocampal neuronal culture as a model system to examine the effect of RNF13 genetic variants on dendritic protein distribution. Our findings offer the first evidence that DEE73-associated RNF13 variants, specifically L311S and L312P, impact neuronal structure.

2. Materials and methods

2.1. Antibodies

The following antibodies were used: Rabbit anti-Rab7 (1:200, Cell Signaling Technology, Cat# 9367, RRID:AB_1904103), Rabbit anti-EEA1 (1:400, Cell Signaling Technology, Cat# 3288, RRID:AB_2096811), Mouse anti-Lamp1 (1:100, Enzo Life Sciences, Cat# ADI-VAM-EN-001, RRID:AB_1082833), Rabbit anti-HA (WB: 1:1000, IF: 1:200, Cell Signaling Technology, Cat# 3724, RRID:AB_1549585), Mouse anti-HA (1:200, BioLegend, San Diego, CA, USA, Cat# 901502, RRID:AB_2565007), Rabbit anti-RCAS1 (1:250, Cell Signaling Technology, Cat# 12290, RRID:AB_2736985), Rabbit anti-MAP2 (1:100, Cell Signaling Technology, Cat #4542, RRID:AB_10693782), Rabbit anti-PSD95 (1:100, Cell Signaling Technology, Cat# 3450, RRID:AB_2292883), Mouse anti-Gephyrin (1:500, Synaptic Systems, Cat# 147 011, RRID:AB_887717), AlexaFluor 488-conjugated Goat anti-Rabbit (1:500, Thermo Fisher Scientific, Cat# A-11034, RRID:AB_2576217), AlexaFluor 488-conjugated Goat anti-Mouse (1:500, Thermo Fisher Scientific, Cat# A-11017, RRID:AB_253408), AlexaFluor 647-conjugated goat anti-mouse (1:500, Thermo Fisher Scientific, Cat# A31626, RRID:AB_2535792), AlexaFluor 647-conjugated goat anti-rabbit (HeLa: 1:1000, Neurons: 1:500, Thermo Fisher Scientific, Cat# A31634) and horseradish peroxidase (HRP)-conjugated goat anti-rabbit (1:10000, Cell Signaling Technology, Cat# 7074, RRID:AB_2099233).

2.2. Molecular biology

GenScript (Piscataway, NJ, USA) synthesized wild-type, full-length human RNF13 transcript variant 1 (accession NM_007282.4), which included the natural Kozak sequence and a C-terminus HA tag. The gene was cloned into pUC57 by *Eco*RV (GenScript). The construct was then used as the template for generating protein variants L311S, L312P, L311A/L312A and C258A/H260A (DN variant) via site-directed mutagenesis. The plasmids were excised using standard enzymatic restriction strategies and ligated using T4 DNA ligase (New England BioLabs Ltd., Cat# M0202) into *Nhe*I and *Xho*I (New England BioLabs Ltd., Cat# R3131 and Cat# R0146, respectively) sites of pCAGGS-IRES-mCherry. The pUC57 vectors of WT, L311S and L312P were used as a template for introducing an optimized Kozak sequence (AACGAG) via PCR performed with Q5 high-fidelity DNA polymerase (New England BioLabs Ltd., Cat# M0492S). The fragments were cleaved using *Bam*HI and *Sal*I (New England BioLabs Ltd., Cat# R3136 and Cat# R3138, respectively) to perform standard ligation into *Bgl*II (New England BioLabs Ltd., Cat# R0144) and *Sal*I sites of the pEGFP-N1 vector. All plasmids were confirmed by Sanger sequencing (Genome Quebec, Montreal, QC, Canada).

2.3. Cell culture and transfection

HEK293T/17 (American Type Culture Collection (ATCC), Gaithersburg, MD, USA, Cat# CRL-11268) and HeLa (from Dr. Diana Alison Averill, Montreal) cells were cultured at subconfluence in Dulbecco's Modified Eagle Medium (DMEM, Thermo Fisher Scientific, Cat# 11995-065) containing 10 % fetal bovine serum (FBS, VWR Life Science, Cat# MPCA97068-085). For maintaining cultures and for the following assays, cells were kept at 37 °C in a humidified atmosphere containing 5 % CO_2. For glycosylation assays, HEK293T/17 cells were transfected with the pCAGGS-IRES-mCherry RNF13-HA vectors in poly-D-lysine-treated,

six-well plates using LipofectAMINE 2000 (Thermo Fisher Scientific, Cat# 11668–019) as described previously (Lussier et al., 2005). Cells were maintained for 48 h before being lysed. For immunostaining assays, 5×10^4 HeLa cells were seeded in a 24-well plate containing a 12 mm round glass coverslip #1.5 (UltiDent Scientific Inc., St-Laurent, QC, Canada, Cat# 170-C12MM) 2 h before transfection. Cells were first transfected with 10 nM DsiRNA using LipofectAMINE 2000 as described previously (Cabana et al., 2021). 48 h later, pEGFP-N1-RNF13 vectors were incorporated using a calcium phosphate-DNA precipitate (Cabana et al., 2021). Cells were maintained for another 24 h before being fixed and processed for immunostaining.

2.4. Neuronal cultures and transfection

Primary neuronal cultures were prepared using Sprague Dawley female rats purchased from Charles River (St-Constant, QC, Canada). The use of timed-pregnant female rats has been approved by the Institutional Animal Care Committee of the University of Quebec at Montreal (CIPA Protocol # 006). Rat hippocampal dissociated neuronal cultures were prepared from embryos of both sexes on day 18 of gestation, as described (Lussier et al., 2012). Dissociated prenatal neurons in Neurobasal culture medium (Thermo Fisher Scientific, Cat# 21,103–049) containing 2 % B-27 Plus supplement (Thermo Fisher Scientific, Cat# A3582801) and 2 mM L-Glutamine (MilliporeSigma, Cat# G7513) were plated on poly-D-lysine-coated 12 mm glass coverslips #1.5 in a 24-well plate at a density of 7.5×10^4 cells per well. They were cultured at 37 °C with a humidified atmosphere containing 5 % CO_2. Transfections were performed at days in vitro (DIV) 4. Briefly, 0.5 µL LipofectAMINE 2000 transfection reagent and 1 µg DNA are separately diluted in 25 µL plain Neurobasal culture medium and incubated for 5 min at room temperature. The two solutions are mixed and incubated for 20 min at room temperature before being added to the cells. Neurons were maintained at 37 °C with 5 % CO_2 before being fixed at DIV10 and processed for immunostaining.

2.5. AP3D1 and AP1G1 knockdown

TriFECTa Kit Dicer-substrate siRNA duplexes against Homo sapiens adaptor-related protein complex 1 subunit gamma 1 (AP1G1, NM_001128) and adaptor-related protein complex 3 subunit delta 1 (AP3D1, NM_003938) were purchased from Integrated DNA Technology (IDT, Coralville, IA) and transfected as described (Cabana et al., 2024). Negative control scrambled dsiRNA (Cat# DS NC1), AP3D1-specific duplex sequences: #1: 5'-rCrGrCrUrArCrUrGrArGrCrArArCrUrUrGrUrUrArGrArAGA-3' and 5'-rUrCrUrUrCrUrArArCrArArGrUrUrGrCrUrCrArGrUrArGrCrGrUrG-3', #2: 5'-rGrUrCrArUrUrUrGrUrUr GrCrGrUrUrGrArArUrUrArUrCTG-3' and 5'-rCrArGrArUrArArUrUrCrArArCrGrCrAr ArCrArArArUrGrArCrCrU-3', AP1G1-specific duplex sequences: #1: 5′-rGrArCrCrUrUrGrArArGrCrArUrUrGrUrUrArArArGrArCTA-3′ and 5'-rUrArGrUrCrUrUrUrArArCrArArUrGrCrUrUrCrArArGrGrUrCrArG-3', #2: 5′-rGrArArArCrGrGrUrUrUrUrGrArCrUrArUrCrArUrGrGrATA-3' and 5′-rUrArUrCrCrArUrGrArUrArGrUrCrArArArArCrCrGrUrUrUrCrArU-3′.

2.6. Immunostaining

Transfected HeLa cells immunostaining was performed as described (Cabana et al., 2024). Transfected neurons were washed with Hanks' Balanced Salt Solution (HBSS) supplemented with Calcium Chloride and Magnesium Chloride (Thermo Fisher Scientific, Cat# 14025–092) before being fixed with ice-cold 4 % paraformaldehyde/4 % sucrose in phosphate-buffered saline (PBS) for 15 min at room temperature. Neurons were permeabilized with 0.25 % Triton X-100 in PBS for 15 min, except when using the Lamp1 antibody that required permeabilization with 0.05 % saponin. Non-specific sites were blocked using 10 % NGS in PBS for 1 h at room temperature (+0.05 % saponin for anti-Lamp1). Coverslips were incubated overnight at 4 °C with the primary antibodies diluted in 3 % NGS/PBS (+0.05 % saponin for anti-Lamp1). Coverslips were washed thoroughly and incubated with the appropriate combinations of AlexaFluor conjugated secondary antibodies diluted in 3 % NGS/PBS (+0.05 % saponin for anti-Lamp1) for 1 h at room temperature. After three washes in PBS, coverslips were mounted using ProLong Diamond Antifade, dried at room temperature overnight and kept at 4 °C until image acquisitions were performed.

2.7. Fluorescence microscopy image acquisition

Image acquisition was performed as described (Cabana et al., 2024). For neurons, the strongest signal was set in the dendrites, although saturation was inevitable in the soma under these conditions. Transfected neurons that were not hippocampal pyramidal cells were excluded from this study, as well as cells that exhibited excessively high or low expression of the ectopic proteins (RNF13) under the selected imaging settings that remained constant within an independent experiment. Some minor lamp intensity and exposure time adjustments were done between independent experiments. The resolution was set at 2048×2048 pixels, and z-stack images were taken at 0.28 µm intervals for 5–12 optical slices. Before analysis, images were deconvoluted using the Olympus 3D Deconvolution feature in the Olympus CellSens Dimension software.

2.8. Image analysis and statistical analysis

For all analyses, a single slice from the middle of a z-stack was analyzed. The two channels were separated to analyze co-localization between RNF13 and endogenous organelle markers, and the threshold was adjusted to have minimal background. Manders overlap coefficients were obtained using the JaCoP plugin in Fiji. To analyze the number of puncta, area covered and the signal intensity of the markers in neurons, a 20 µm section of three dendrites from 10 neurons per independent experiment was chosen at 50 µm from the soma or directly adjacent to the soma. Specifically, using a scale bar, 20 µm horizontal and vertical rectangles were saved in the ROI manager. Dendrites that were straight in the rectangle were chosen to ensure they were 20 µm long. The section was duplicated and saved as a new image. ROI was drawn on each side of the dendrites to remove the signal from neighboring neurites. The channels were split, Fiji's "Default" threshold was applied, and both Fiji's Analyze particles and Measure functions were used. The integrated density obtained was then normalized against the control (NT) average for one independent experiment to consider possible lamp intensity and exposure time variations during image acquisition. At least three independent, non-blinded experiments were performed for all assays. Datasets were collected in Microsoft Excel before being subjected to statistical analysis in GraphPad Prism 10. Statistical difference was determined using either repeated measure (RM) one-way ANOVA or two-way ANOVA when there are one or two grouping variables, respectively. Both are analyzed using the Geisser-Greenhouse correction and Dunnett's multiple comparisons test. Relevant data can be found in the article and its supplementary material.

2.9. Cell lysis and glycosylation assays

Transfected HEK293T/17 cells were washed with PBS and lysed in 1 mL ice-cold RIPA lysis buffer (20 mM Tris-HCl pH 7.5, 150 mM NaCl, 1 % Triton X-100, 5 mM EDTA, 0.1 % sodium dodecyl sulfate (SDS), 0.5 % sodium deoxycholate and 1X EDTA-free protease inhibitor cocktail (Bimake.com, Houston, TX, USA, Cat# B14001)). Lysates were agitated at 15 rpm for 20 min at 4 °C before being centrifuged at maximum speed (~21,100 x g) for 15 min. 500 µL of diluted 1:1 lysate in RIPA buffer was agitated at 15 rpm overnight at 4 °C with 10 µL of anti-HA magnetic beads (Bimake.com, Houston, TX, USA, Cat# B26201) pre-equilibrated in 0.25 % Triton X-100 in PBS (PBS-T). After three 5 min

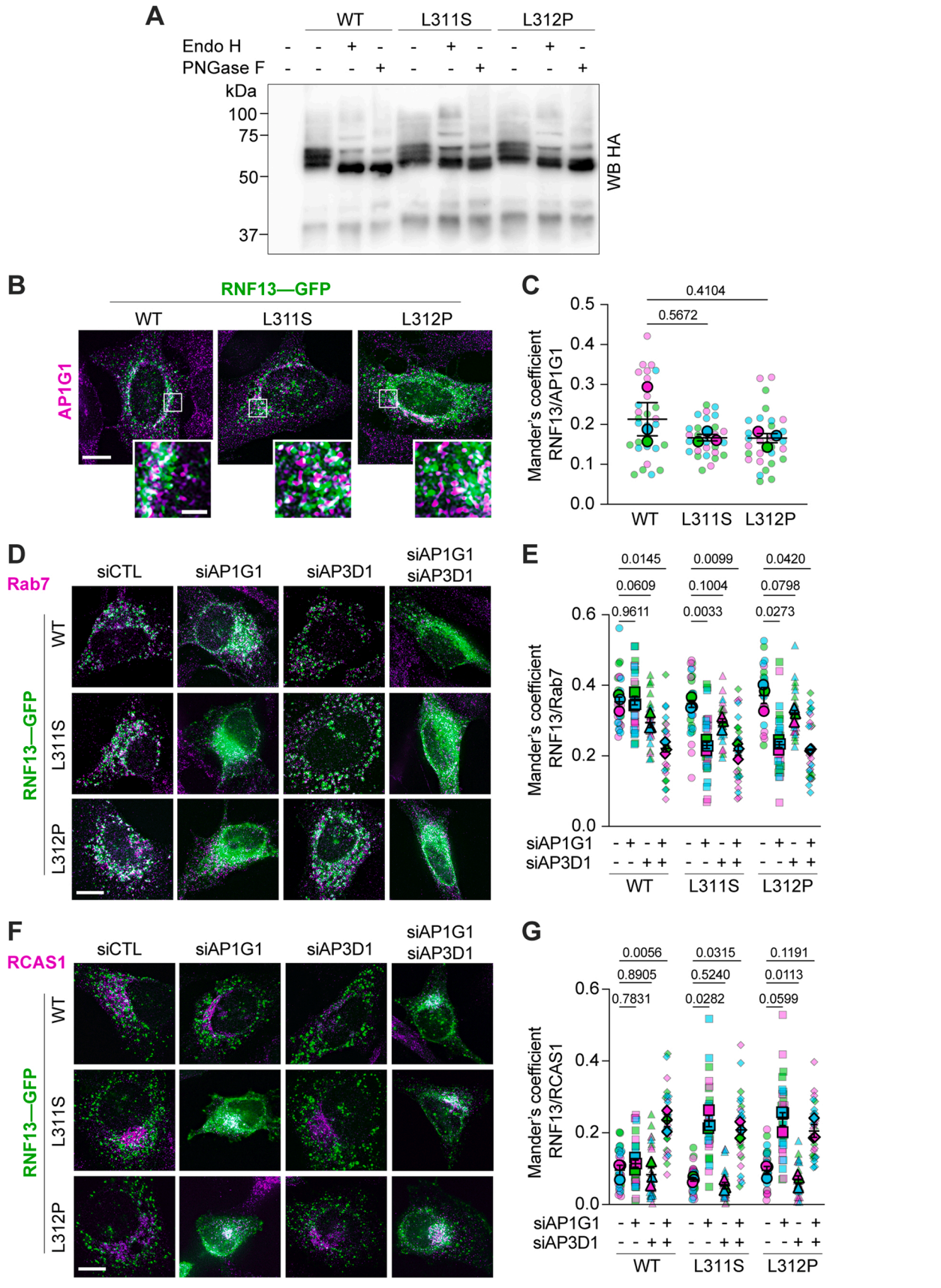

(caption on next page)

Fig. 1. RNF13 variants L311S and L312P use an AP-1-dependent pathway for endosomal targeting. (A) Representative immunoblot from three independent experiments (N = 3) of immunoprecipitated HA-tagged RNF13 (WT, L311S and L312P) digested with Endo H or PNGase F. (B) Representative immunofluorescence images show HeLa cells expressing RNF13-GFP (in green) and endogenous AP1G1 (in purple). Scale bars indicate 10 μm for the whole cell image and 2 μm for the boxed areas shown in higher magnification. (C) The jittered individual value plots represent Manders' overlap coefficient of RNF13 over AP1G1. (D-G) Representative images show RNF13-GFP (in green) and endogenous staining (in purple) of (D) late endosome marker Rab7 or (F) Golgi marker RCAS1 of DsiRNA-transfected HeLa cells. Scale bars indicate 10 μm for the whole cell image and 2 μm for the boxed areas shown in higher magnification. The jittered individual value plots represent Manders' overlap coefficient of RNF13 over (E) Rab7 and (G) RCAS1. (C, E, G) Values are expressed as mean ± SEM. Each color represents an independent experiment, with smaller points representing the data for each cell (n = 30 cells) and larger points representing the mean of an independent experiment (N = 3). For each condition analyzed (N = 3), statistical analysis was conducted using RM two-way ANOVA with the Geisser-Greenhouse correction and Dunnett's multiple comparisons test with individual variances computed for each comparison.

washes with PBS-T, immunopurified proteins were incubated at 100 °C for 10 min in 1x Glycoprotein Denaturing Buffer (New England Biolabs, Beverly, MA, USA, Cat# P0703S). Proteins were then digested with 500 U of Endo Hf (New England Biolabs, Beverly, MA, USA, Cat# P0703S) or PNGase F (New England Biolabs, Beverly, MA, USA, Cat# P0704S) for 2 h at 37 °C before stopping the reaction with Laemmli buffer and loading on SDS-PAGE.

2.10. SDS-PAGE and western blot

Protein samples were separated on a 1.5 mm SDS-PAGE gel containing 0.5 % of 2,2,2-trichloroethanol (TCE). Non-specific sites were blocked using 5 % skim milk in TBS-T (20 mM Tris-HCl pH 7.5, 140 mM NaCl, 0.3 % Tween-20) for 1 h at room temperature. Membranes were incubated with primary antibodies diluted in TBS-T supplemented with 0.05 % NaN_3 overnight at 4 °C then thoroughly washed with TBS-T. At room temperature, incubation with horseradish peroxidase-coupled secondary antibodies diluted in TBS-T was performed for 1 h. After thoroughly washing the membranes with TBS-T, immune complexes were revealed using the Clarity Western ECL substrate (BioRad, Cat# 1705060) using the ChemiDoc MP imaging system.

3. Results

3.1. RNF13 variants L311S and L312P traffic through an AP-1-dependent pathway

In our previous work, we reported that AP-3 knockdown caused the improper lysosomal localization of RNF13 WT, which resulted in the enlargement of endosomal vesicles (Cabana et al., 2021). Moreover, L311S and L312P variants, as well as a variant lacking the dileucine residues (L311A/L312A, henceforth designated LL/AA), fail to interact with the AP-3 complex (Cabana et al., 2021). The presence of these variant proteins in lysosomes was markedly reduced, although still localized to late endosomes (Cabana et al., 2021). To gain further insight into the trafficking of variants through the biosynthetic secretory pathway and the potential impact on glycosylation, we performed endoglycosidase H (Endo H) and peptide-N-glycosidase F (PNGase F) digestion. HA-tagged RNF13 proteins (WT, L311S and L312P) expressed in HEK293T/17 cells were immunoprecipitated. The results show that undigested RNF13 WT had three intense immunodetected protein species at approximately 53, 58 and 62 kDa, two fainter bands around 38 and 43 kDa, and two faint bands at 72 and 80 kDa (Fig. 1A). Digestion with Endo H resulted in a reduction of the 62 kDa band. At the same time, band at 50 kDa became RNF13's most abundant species (Fig. 1A). In contrast, the 50 kDa band shifted to around 48 kDa when digested with PNGase F (Fig. 1A). Importantly, both L311S and L312P variants displayed the same, reproducible patterns as the WT protein (Fig. 1A), suggesting that these variants traffic normally through the biosynthetic pathway.

L311S and L312P variants display normal late endosomal localization and altered lysosomal localization compared to RNF13 WT. Thus, another sorting signal and pathway likely contribute to their late endosome targeting. Accordingly, RNF13 LL/AA is trafficked from the TGN toward the endosomes through an AP-1-dependent pathway by interacting with a second motif in RNF13's C-terminus (Cabana et al., 2024). A non-canonical VVVQLQ motif allows RNF13 interaction with AP1M1 but not AP3M1 (Cabana et al., 2024). We wondered whether the endosomal localization of variants L311S and L312P could be accomplished through an AP-1-dependent pathway since this second motif remains intact within both variants. To confirm this hypothesis, an immunofluorescence-based co-localization assay between RNF13 and AP1G1 was performed. HeLa cells were transfected with plasmids encoding GFP-tagged RNF13 WT, L311S and L312P proteins. The endogenous AP1G1 subunit was labelled using a specific primary antibody. The results show that signal overlap is similar in all conditions, as demonstrated by no significant difference in the Manders overlap coefficient for WT, L311S and L312P over AP1G1 (Fig. 1B-C).

We then assessed whether the L311S and L312P variants require the AP-1 complex to reach the endosomal compartment. HeLa cells were transfected with siCTL, siAP1G1, siAP3D1 or the previously validated combination of siAP1G1 and siAP3D1 for 72 h (Cabana et al., 2024). 24 h before labelling with endogenous subcellular markers Rab7 or RCAS1 (Receptor-binding cancer antigen expressed on SiSo cells), cells were transfected with plasmids encoding GFP-tagged RNF13 WT, L311S or L312P proteins. The results showed a partial overlap between RNF13 WT and Rab7 when the AP complexes are repressed individually, whereas this overlap significantly decreases when AP1G1 and AP3D1 are knocked down (Fig. 1D-E). The repression of AP3D1 did not affect RNF13 L311S or L312P late endosomal localization. This contrasts with AP1G1 knockdown that significantly decreased the overlap between Rab7 and the L311S and L312P variants (Fig. 1D-E).

To determine whether knocking down AP-1 or AP-3 led to a retention of L311S and L312P variants in the Golgi apparatus, HeLa cells were transfected with specific siRNA, transfected with RNF13 WT or variants, and immunolabeled to detect RCAS1. The knockdown of AP1G1 alone was sufficient to increase Manders' coefficient between RNF13 variants L311S and L312P and RCAS1, although the increase for L312P did not reach statistical significance (Fig. 1F-G). In contrast, the combination with AP3D1 knockdown was necessary to obtain similar results for the WT protein (Fig. 1F-G). These results suggest that RNF13 variants L311S and L312P are trafficked through an AP-1-dependent pathway to exit the Golgi and reach the endosomal compartment.

3.2. Increased presence of RNF13 variants in dendrites

While there is some redundancy in the functions of AP-1 and AP-3 complexes in most cells, they are important for compartmental complexity in neurons (Guardia et al., 2018). AP-1 is responsible for sorting proteins from the TGN and endosomes toward the somatodendritic domain while AP-3 sorts proteins from endosomes toward the axon and is involved in SV biogenesis (Guardia et al., 2018). As RNF13 L311S and L312P were reported to cause severe neurological symptoms (Edvardson et al., 2019) and only traffic through an AP-1-dependent pathway (Fig. 1), we wondered if they might be unevenly distributed in the somatodendritic domain, which could lead to synaptic dysfunction. To assess their localization in neurons, rat primary cultures of hippocampal neurons were transfected with plasmids encoding HA-tagged RNF13 (WT, L311S and L312P) proteins at day in vitro (DIV) 4. As variants of RNF13 cause an infantile neurodegenerative disease,

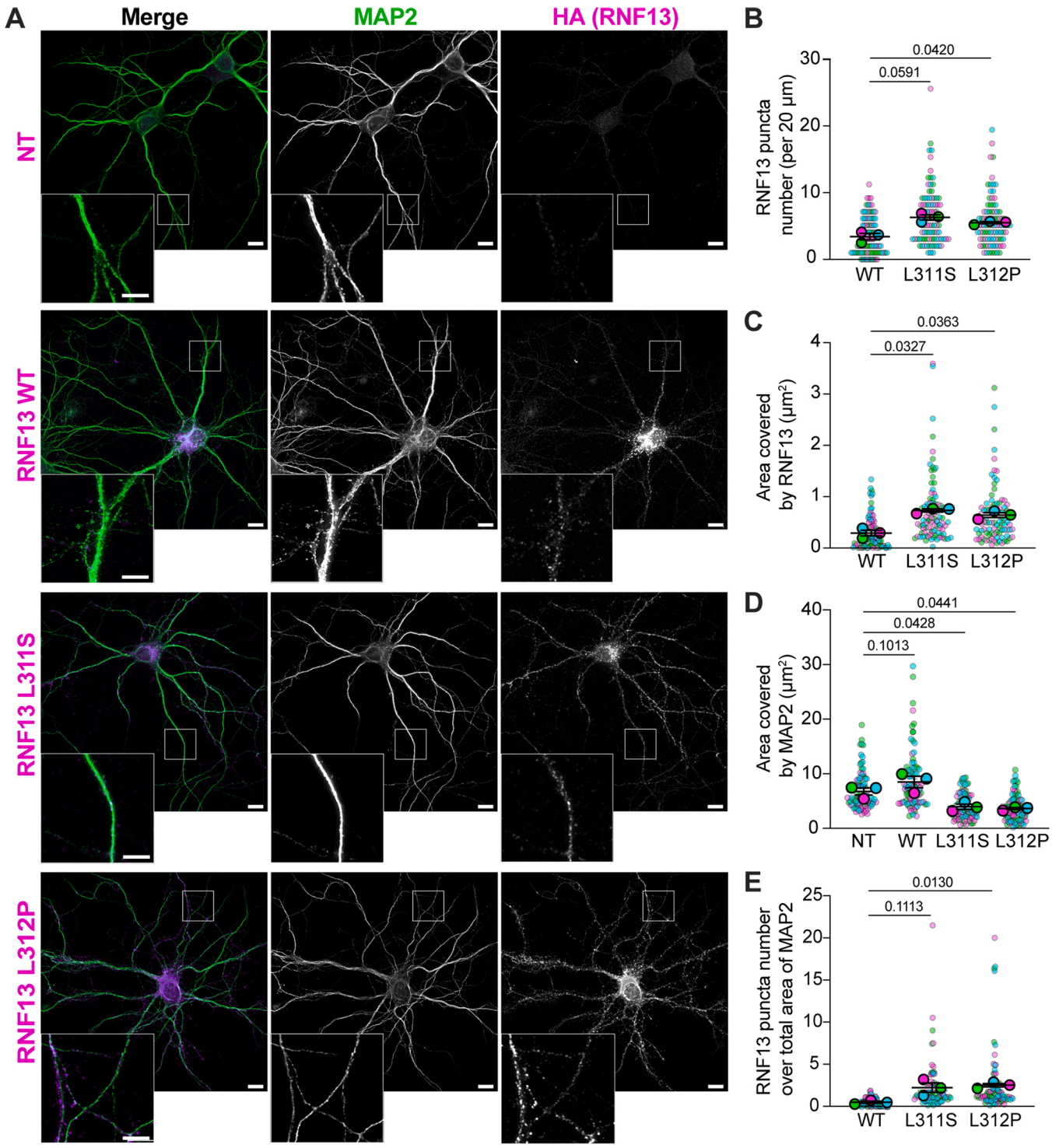

Fig. 2. RNF13 variants L311S and L312P show increased localization in dendrites and alter their morphology. (A) Representative images of primary cultures of hippocampal neurons transfected at DIV4 with HA-tagged RNF13 (WT, L311S and L312P) proteins encoding plasmids or empty vector and fixed at DIV10 show the staining of RNF13-HA (in purple) and endogenous dendrites marker MAP2 (in green). Scale bars indicate 10 µm for the whole cell image and 5 µm for the boxed areas shown in higher magnification. The jittered individual value plots represent the (B) number of RNF13 puncta, (C) area covered by RNF13 staining, (D) area covered by MAP2 staining, and (E) the number of RNF13 puncta normalized over the total area of MAP2 in a 20 µm dendrite section taken 50 µm away from the soma. Values are expressed as mean ± SEM. Each color represents an independent experiment where smaller points represent each dendrite analyzed (n = 90 dendrites), and larger points represent the mean of an independent experiment (N = 3). For each condition analyzed, N = 3 was used for RM one-way ANOVA with the Geisser-Greenhouse correction, and Dunnett's multiple comparisons test with individual variances was calculated for each comparison.

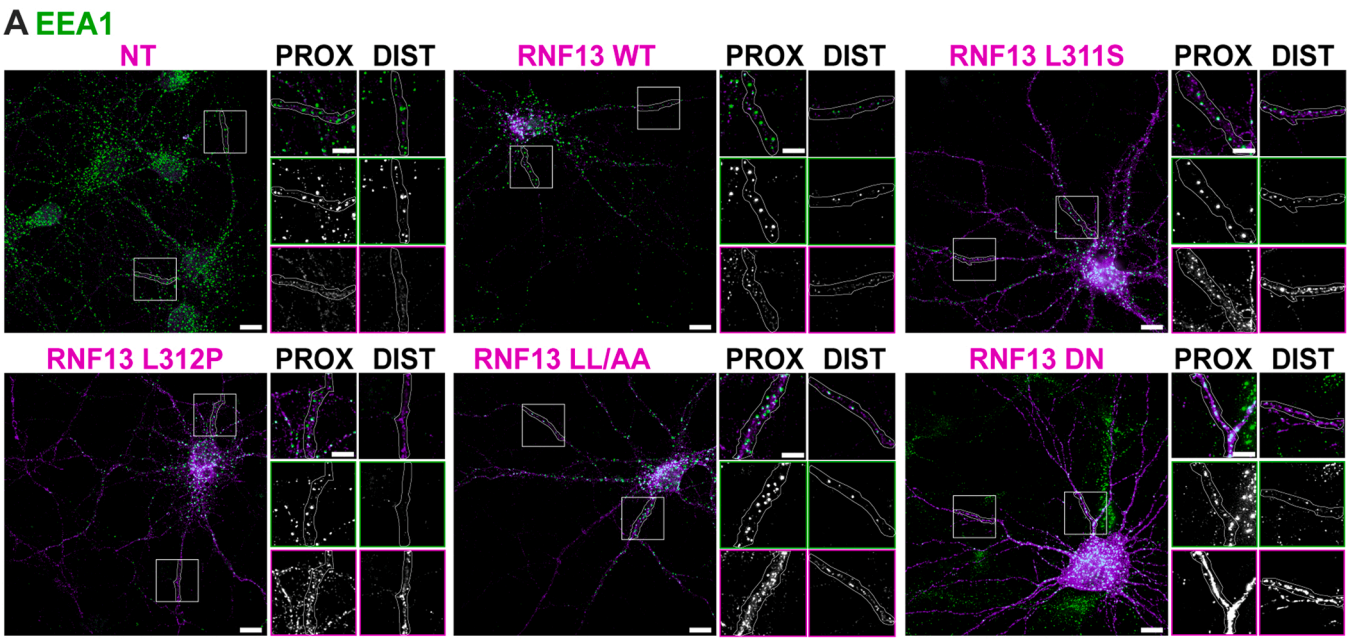

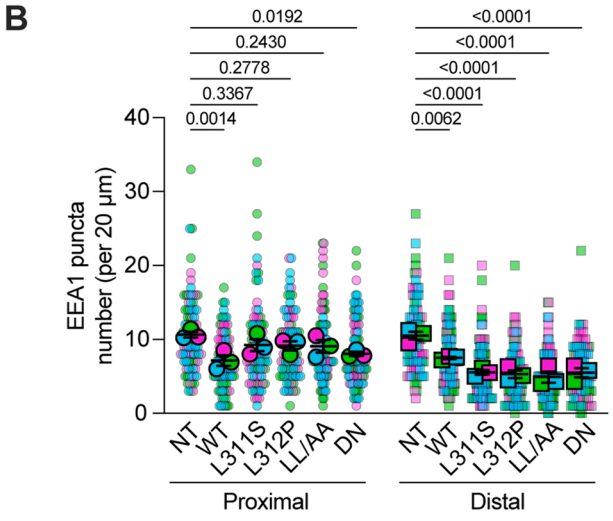

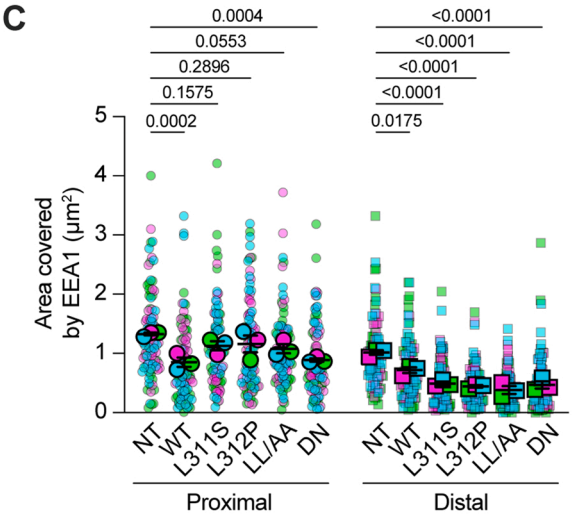

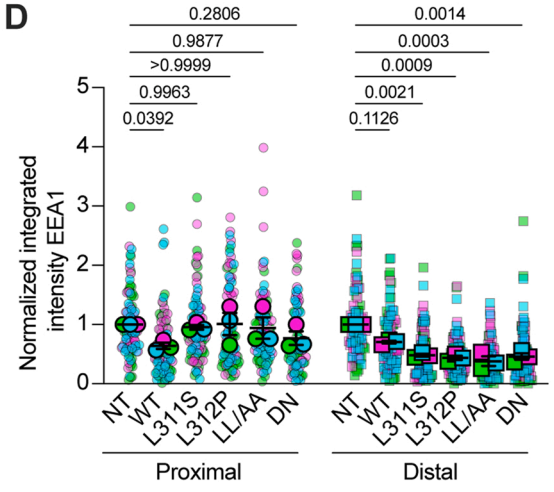

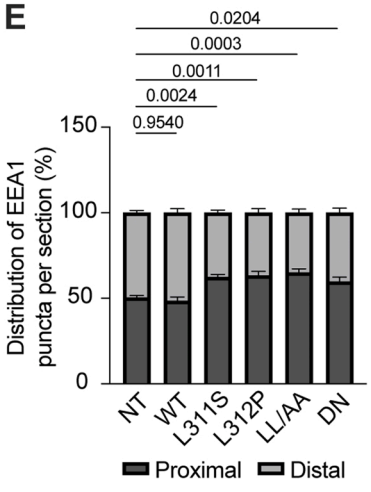

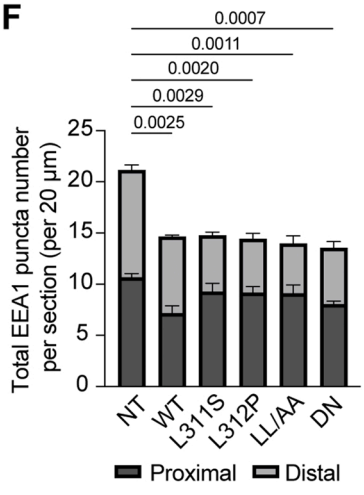

(caption on next page)

Fig. 3. Alterations in the dileucine motif and the Ub ligase catalytic site change the distribution of early endosomes in dendrites. Primary cultures of hippocampal neurons transfected at DIV4 with an empty vector or plasmids encoding HA-tagged RNF13 (WT, L311S, L312P, LL/AA and DN) proteins were fixed at DIV10. (A) Representative images show the staining of RNF13-HA (in purple) and endogenous early endosome marker EEA1 (in green). Scale bars indicate 10 μm for the whole cell image and 5 μm for the boxed areas shown in higher magnification (green boxes for EEA1, purple boxes for RNF13), where the channels are presented as merged (top) or individually separated. PROX, proximal section, DIST, distal section. The jittered individual value plots represent the (B) number, (C) area covered, and (D) normalized signal intensity of EEA1 in a 20 μm dendrites section taken directly after (proximal) or 50 μm away (distal) from the soma. Each color represents an independent experiment where smaller points represent each dendrite analyzed (n = 90 dendrites), and bigger points represent the mean of an independent experiment (N = 3). The summary bar plots represent the proportion of EEA1 in the proximal and distal sections (E) and the total number of EEA1 in both sections (F). The data are presented as mean ± SEM and were subjected to statistical analysis using RM two-way ANOVA with the Geisser-Greenhouse correction and Dunnett's multiple comparisons test with a single pooled variance. This compares the simple effects within columns (B-E) and the mean row effect (F).

neurons were transfected early in development and fixed at DIV10 for immunofluorescence staining to allow potential defects to develop during neuronal growth. Endogenous Microtubule-associated protein 2 (MAP2) was immunolabelled using a specific antibody to detect dendrites, and RNF13 was detected using an anti-HA antibody. RNF13 WT localized in the soma and primary dendrites (Fig. 2A). In contrast, both variants L311S and L312P extend to secondary and tertiary dendrites, much further from the soma than the WT (Fig. 2A). Quantitation of RNF13 presence in a section of distal dendrite positioned 50 μm away from the soma show increase of the variants L311S and L312P when compared to WT (Fig. 2B). Furthermore, the area covered by RNF13 staining was significantly higher for both variants when compared to the WT protein (Fig. 2C). Interestingly, we observed that the dendrites appeared thinner in the presence of the variants, which was supported by a decreased MAP2-staining area for both L311S and L312P when compared to a non-transfected neuron (NT) (Fig. 2D). Because the dendrites expressing RNF13 WT were larger while having a smaller count of RNF13, the ratio of L311S and L312P RNF13 puncta over the MAP2 area were higher than for WT RNF13, although L311S did not reach statistical significance (Fig. 2E). Together, these results suggest that an increased concentration of L311S and L312P variants in proximal dendrites alter dendritic morphology.

3.3. Alterations in the dileucine motif act as a dominant negative and redistribute early endosomes in dendrites

The importance of the endolysosomal system is well-established for proper synaptic function (Winckler et al., 2018; Grochowska et al., 2022). We have previously demonstrated that epidermal growth factor (EGF) progression was altered at the early endosome by RNF13 L311S and L312P variants and modification to the dileucine motif caused the enlargement of early endosome antigen 1 (EEA1)-positive vesicles in HeLa cells (Cabana et al., 2021). Based on these results, we wondered if the variants would affect early endosomes in neurons. Because it was suggested that L311S might add a phosphorylation site and that L312P might increase the probability of phosphorylation to an adjacent threonine (Edvardson et al., 2019), we used the previously characterized AP-3-binding defective variant LL/AA as a control to understand the importance of the dileucine motif and proper trafficking of RNF13 (Cabana et al., 2021; Cabana et al., 2024). Furthermore, given that RNF13 E3 Ub ligase activity is involved in most of its reported function (Zhang et al., 2009; Arshad et al., 2013; Zhang et al., 2013; Miyakawa et al., 2022; Lin et al., 2023; Liu et al., 2024), we compared the dileucine-altered variants' phenotypes to the dominant negative (hereafter named DN) version of RNF13 as previously characterized (Zhang et al., 2009; Zhang et al., 2013; Lin et al., 2023).

To study how RNF13 variants affect early endosomes in dendrites, we transfected cultures of rat primary hippocampal neurons with plasmids encoding HA-tagged RNF13 (WT, L311S, L312P, LL/AA and DN) proteins at DIV4. Fixation and immunolabeling of endogenous early endosomes were performed at DIV10 using an EEA1-specific antibody. A 20 μm section of dendrite was drawn either directly after the soma (PROX, left zoom) or 50 μm away from the soma (DIST, right zoom) to quantify EEA1 presence in each section (Fig. 3A). The presence of RNF13 WT and DN significantly decreased the number of EEA1 puncta in the proximal dendrites while the dileucine-altered variants had a minor and insignificant effect compared to NT (Fig. 3B). However, in distal dendrites, the DN variant decreased EEA1 puncta number to a level similar to L311S, L312P and LL/AA, while RNF13 WT had an intermediate phenotype (Fig. 3B).

To circumvent a potential underestimation of EEA1 presence due to differences in puncta size, we compared the area covered by EEA1 staining. The results show that the area covered by EEA1 staining decreased in proximal dendrites expressing WT and DN RNF13 compared to NT cells (Fig. 3C). In distal dendrites, the expression of RNF13 WT and variants significantly reduced the area covered by EEA1 when compared to NT (Fig. 3C). An important limitation of our methodology is the level of resolution that can be achieved with deconvoluted epifluorescence microscopy images. Puncta are thus more accurately described as clusters of proteins, given that the fluorescence intensity is proportional to the protein abundance. The difference in fluorescence intensity was significantly decreased for the WT in the proximal dendrites but not in the distal dendrites (Fig. 3D). In contrast, whereas the variants did not modify EEA1 fluorescence intensity in the proximal dendrites, they significantly altered EEA1-linked fluorescence in distal dendrites (Fig. 3D). The results also showed that all variants significantly impact the proportion of EEA1 puncta number in proximal and distal dendrites, whereas no significant modification was measured between WT and NT cells (Fig. 3E). Furthermore, when the number of EEA1 puncta in both sections was added to enable comparison, all variants exhibited values comparable to those of the WT, which were significantly lower than those of the NT (Fig. 3F). Overall, these results show that the variants disrupted the spatial distribution of early endosomes, indicating that there may be a defect in the transport mechanism in dendrites.

3.4. Lysosome number is decreased in proximal dendrites in the presence of RNF13

A recent study implicated RNF13 in lysosomal acidification (Liu et al., 2024). Our work shows that RNF13 is higher in late endosomes and lysosomes than in early endosomes, and that RNF13 dileucine variants are not correctly targeted to lysosomes (Cabana et al., 2021). RNF13 L311S and L312P variants may also affect lysosomes in neurons. To determine whether RNF13 variants affect the distribution of lysosomes in dendrites, primary cultures of rat hippocampal neurons were transfected at DIV4 with plasmids encoding HA-tagged RNF13 (WT, L311S, L312P, LL/AA and DN) proteins. At DIV10, fixation and subsequent immunolabeling was performed against HA and endogenous Lamp1. As previously described, a 20 μm section of dendrite was drawn either in direct proximity to the soma (PROX, left zoom) or 50 μm away from the soma (DIST, right zoom) (Fig. 4A). RNF13 WT and all the variants significantly decreased Lamp1 puncta number in proximal dendrites (Fig. 4B). In contrast, no difference was observed in distal dendrites although the WT presented a slight but not significant increase (Fig. 4B). The area covered by Lamp1 and its fluorescence intensity declined, but the fluorescence intensity in proximal dendrites did not reach statistical significance (Fig. 4C-D). No statistical differences were measured for WT or variants RNF13 in the distal dendrites. (Fig. 4C-D). Unexpectedly, only RNF13 WT significantly altered the proportion of

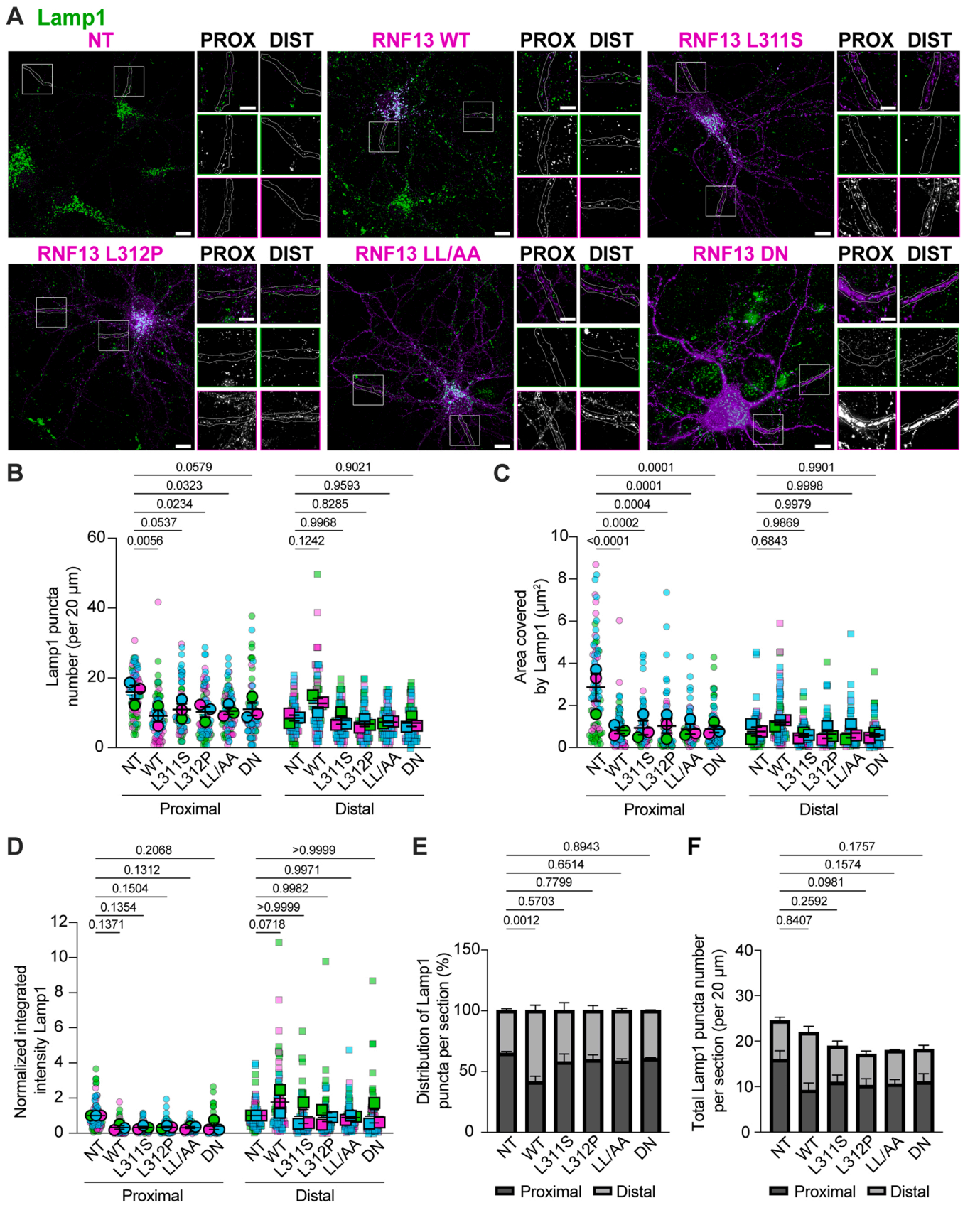

(caption on next page)

Fig. 4. The number of Lamp1-positive lysosomes is reduced in the proximal dendrites of neurons expressing RNF13 whereas only WT RNF13 alter their distribution. (A) Representative images show RNF13-HA (in purple) and staining of endogenous lysosome marker Lamp1 (in green) in primary cultures of hippocampal neurons transfected at DIV4 with HA-tagged RNF13 (WT, L311S, L312P, LL/AA and DN) proteins encoding plasmids or empty vector and fixed at DIV10. Scale bars indicate 10 μm for the whole cell image and 5 μm for the boxed areas shown in higher magnification (green boxes for Lamp1, purple boxes for RNF13), where channels are presented as merged (top) or individually separated. PROX, proximal section, DIST, distal section. The jittered individual value plots represent the (B) number, (C) area covered, and (D) normalized signal intensity of Lamp1 in a 20 μm dendrites section taken directly after (proximal) or 50 μm away (distal) from the soma. Each color represents an independent experiment where smaller points represent each dendrite analyzed (n = 90 dendrites), and bigger points represent the mean of an independent experiment (N = 3). The summary bar plots represent the proportion of Lamp1 for the proximal and distal sections (E) and the total number of Lamp1 in both sections (F). The results are presented as mean ± SEM. The data were subjected to statistical analysis using RM two-way ANOVA with the Geisser-Greenhouse correction and Dunnett's multiple comparisons test with a single pooled variance to compare (B-E) simple effects within columns and (F) the mean row effect.

Lamp1 puncta number found in each section (Fig. 4E). In comparison, the presence of L311S, L312P, LL/AA and DN variants had no significant effect in the proximal dendrites (Fig. 4E). The total number of Lamp1 puncta in both sections was not significantly different although a slight decrease was measured for the four variants (Fig. 4F). Given that the proximal lysosomes are known to be the most degradative (Yap and Winckler, 2022), the results suggest that the presence of RNF13 variants might alter lysosomal maturation in neurons, while the WT variant appears to redistribute the lysosomes towards distal dendrites.

3.5. *RNF13 WT increases the number of PSD-95 particles in distal dendrites*

It is reported that inhibition of lysosomes reduces the number of spines and that the trafficking of lysosomes in distal dendrites is highly correlated with synaptic activity (Goo et al., 2017). It is also established that spine morphology is closely linked to synaptic function. Furthermore, numerous neurodegenerative and neurodevelopmental diseases display alterations in dendritic spines (Penzes et al., 2011; Nishiyama, 2019; Nelson and Bender, 2021). To gain a deeper understanding of the potential impact of RNF13 variants on the development of dendritic spines in excitatory neurons, we assessed PSD-95 abundance. PSD-95 is an important protein that plays a role in the trafficking, localization and anchoring of glutamate receptors (Yoo et al., 2019). At DIV4, rat primary hippocampal cultures were transfected with plasmids encoding HA-tagged RNF13 (WT, L311S, L312P, LL/AA and DN) proteins. At DIV10, when neurons are still at an early stage of their development, endogenous labelling was performed using a PSD-95-specific antibody. As previously outlined, a 20 μm section of dendrite was selected either directly after the soma (PROX, left zoom) or 50 μm away from the soma (DIST, right zoom) (Fig. 5A). When compared to NT in distal dendrite, the number, area and fluorescence intensity of PSD-95 puncta were significantly increased by the presence of RNF13 WT but not by any of the variants (Fig. 5B-C-D). In proximal dendrites, only the L311S variant significantly decreased the area and fluorescence intensity (Fig. 5B-C-D). As there was a significant increase in one section but not the other, RNF13 WT also significantly changed the proportion of PSD-95 found in each section (Fig. 5E). However, the total number of PSD-95 particles increased but did not reach statistical significance for the WT while all the variants had no effect (Fig. 5F). It is important to note that PSD-95 is present as puncta before spines form (Gerrow et al., 2006), and that DIV10 is still early to detect fully mature spines or synapses (Barnes and Polleux, 2009). In this context, the results suggest that RNF13 affects the development of excitatory synapses and requires both the dileucine motif and the Ub ligase catalytic site for this phenotype.

3.6. *Dileucine-altered variants decrease gephyrin abundance in dendrites*

The RNF13 L311S and L312P variants were reported to cause refractory seizure in affected individuals (Edvardson et al., 2019). It is well documented that an impairment in inhibitory neurotransmission may be a contributing factor in the occurrence of seizures (Dzyubenko et al., 2021; Platzer et al., 2022; Guerrini et al., 2023). Given the observed differences in dendrite morphology and PSD-95 abundance, we sought to determine whether inhibitory synaptic sites are also affected by the presence of RNF13. We examined Gephyrin, a protein that anchors, clusters and stabilizes glycine and gamma-aminobutyric acid (GABA) receptors at inhibitory synapses (Choii and Ko, 2015). Again, HA-tagged RNF13-expressing cultures of rat primary hippocampal neurons were fixed at DIV10 and immunolabeled using a specific antibody against Gephyrin. A 20 μm section of dendrite near the soma (PROX, left zoom) and 50 μm away from the soma (DIST, right zoom) were selected for analysis (Fig. 6A). The number of puncta was significantly reduced only in the distal section for all the variants (Fig. 6B). The area covered by Gephyrin staining was not affected in proximal dendrites, but it was significantly decreased in the distal section by the presence of the L311S, L312P and LL/AA variants (Fig. 6C). In addition, only RNF13 L311S, L312P and LL/AA decreased the fluorescence intensity of Gephyrin in distal dendrites with no effect observed in the proximal section (Fig. 6D). The proportion of Gephyrin puncta number in each segment (i.e proximal vs distal) was not significantly different for any condition (Fig. 6E). Notably, only the dileucine-altered variants resulted in a significant decrease in the total number of Gephyrin puncta (Fig. 6F). Together, these findings indicate that the RNF13 dileucine motif plays a role in the development of inhibitory synapses, whereas the RNF13 E3 ligase catalytic site exerts a partial influence on the cellular mechanism involved (Fig. 7).

4. Discussion

Neurons are highly polarized cells with an important compartmental complexity, which allows AP complexes to achieve different and specific functions (Guardia et al., 2018; Donato et al., 2019). The differential binding affinity of cargo proteins to either AP-1 or AP-3 complexes enables the targeted delivery of materials to dendritic or axonal locations, respectively (Li et al., 2016). In the nematode *C. elegans*, the dileucine motif (ETKPLI) in the axonal G-protein coupled serotonin receptor/SER-1 is preferentially bound to AP-3. In contrast, the receptor tyrosine kinase CAM-1 has two dileucine motifs (DNSLL and DLHELL), which are crucial for its dendritic targeting and preferential binding to AP-1 (Li et al., 2016). Substituting the SER-1 dileucine motif with those found in CAM-1 resulted in a change in SER-1 localization from axonal to dendritic (Li et al., 2016). While evaluating RNF13's preferential AP complex binding is beyond the scope of this study, the fact that the variant proteins only traffic through an AP-1-dependent pathway may result in an important redistribution of the protein, which could explain their increased presence in the somatodendritic domain (Figs. 1 and 2).

The spatial regulation of different cellular compartments is critical to ensure proper proteostasis (Grochowska et al., 2022). In neurons, early endosome particles are distributed throughout the dendrites and exhibit minimal movement compared to late endosome particles, which display bidirectional mobility (Yap and Winckler, 2022). Specifically, Rab7 is recruited and activated at early endosome membranes, converting them into motile late endosomes (Yap et al., 2022). Notably, early endosomes were distributed uniformly throughout the dendrites when RNF13 WT was present (Fig. 3). However, all the variants altered this distribution, increasing the number of EEA1-positive early endosomes proximal to the soma and a decrease in distal dendrites (Fig. 3). Given the limited mobility of early endosomes, this observation points to a potential defect in the retrograde transport of late endosomes in the dendrites. In

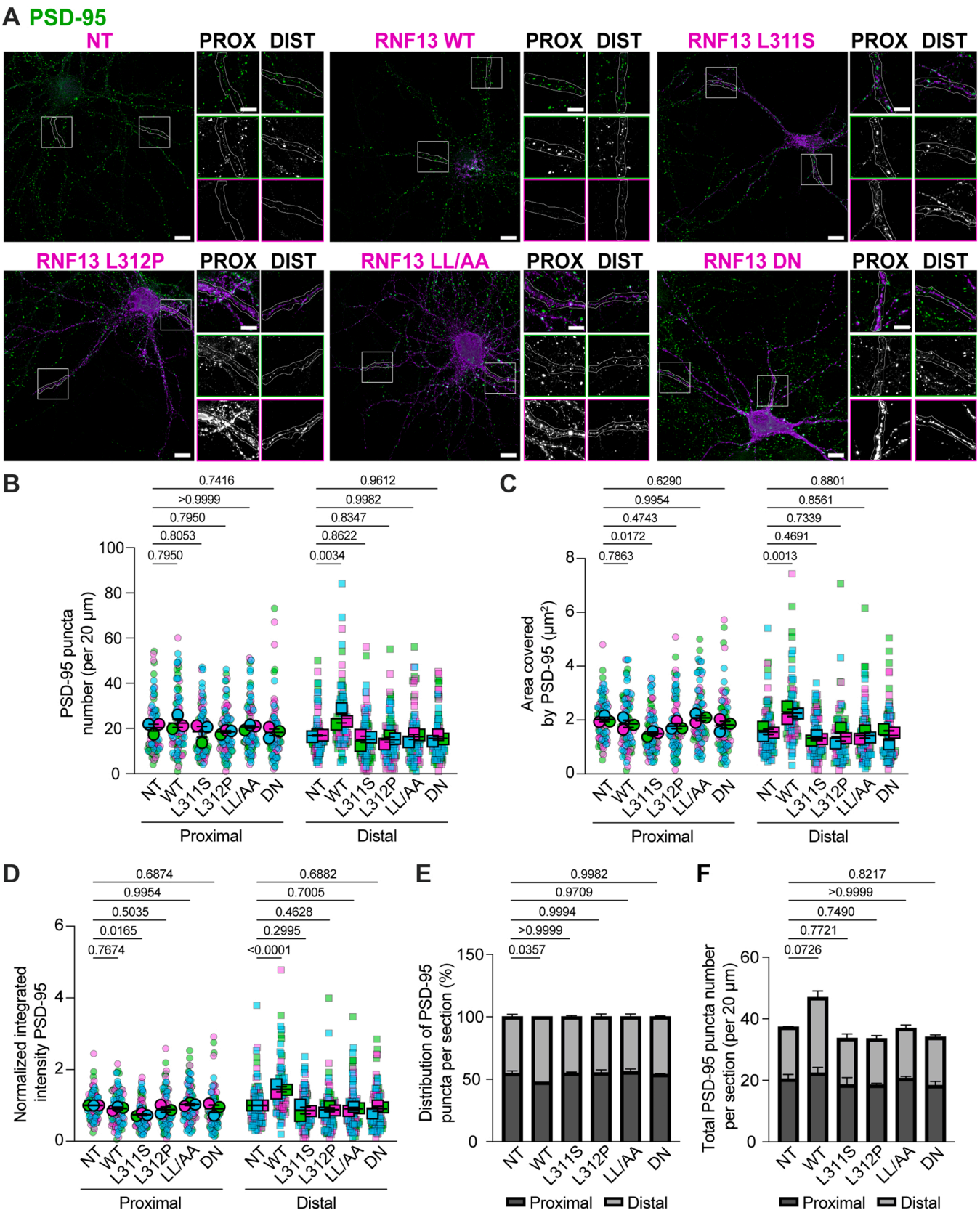

(caption on next page)

Fig. 5. An intact dileucine motif and Ub ligase activity of RNF13 are required to increase PSD-95 abundance in proximal dendrite. Primary cultures of hippocampal neurons were transfected at DIV4 with HA-tagged RNF13 (WT, L311S, L312P, LL/AA and DN) protein-encoding plasmids or an empty vector and fixed at DIV10. (A) Representative images show the staining of RNF13-HA (in purple) and endogenous excitatory synapse marker PSD-95 (in green). Scale bars indicate 10 μm for the whole cell image and 5 μm for the boxed areas shown in higher magnification (green boxes for PSD-95, purple boxes for RNF13), where the channels are presented as merged (top) or individually separated. PROX, proximal section, DIST, distal section. The jittered individual value plots represent the (B) number, (C) area covered, and (D) normalized signal intensity of PSD-95 in a 20 μm dendrites section taken directly after (proximal) or 50 μm away (distal) from the soma. Each color represents an independent experiment where smaller points represent each individual dendrite analyzed (n = 90 dendrites) and bigger points represent the mean of an independent experiment (N = 3). The summary bar plots represent the proportion of PSD-95 in the proximal and distal sections (E) and the total number of PSD-95 in both sections (F). Analyzed values are expressed as mean ± SEM and analyzed using RM two-way ANOVA with the Geisser-Greenhouse correction and Dunnett's multiple comparisons test with a single pooled variance to compare (B-E) simple effects within columns and (F) the mean row effect.

addition, defective retrograde transport results in alterations to dendritic morphology (Cai et al., 2010), which could be the underlying cause of the reduced MAP2-covered area observed in the presence of L311S and L312P (Fig. 2). Although highly speculative, a potential mechanism could involve alterations in retrograde transport, allowing Rab7 to accumulate and consequently only perform the early-to-late endosome switch distally. Given that highly degradative dendritic lysosomes are predominantly within the initial 25 μm from the soma (Yap and Winckler, 2022), an altered maturation in proximal dendrites would be consistent with the observed combination of increased EEA1 and decreased Lamp1 presence across all variants (Figs. 3, 4).

RNF13 gene expression was shown to be expressed at a higher level following stimulation of the substrate adhesion molecule Cytotactin/Tenascin-C (Tranque et al., 1996), and its staining was also correlated with Tenascin-C expression, an important extracellular matrix (ECM) proteoglycan (Zhang et al., 2009). In addition, RNF13 enhances Matrix metalloproteinase-9 (MMP-9) activity via an E3 ligase-dependent mechanism (Zhang et al., 2009). Although the precise cellular mechanisms remain to be elucidated, the evidence suggests that RNF13 plays a role in the ECM. It is known that the brain's ECM is a crucial regulator of synapses (Dzyubenko et al., 2021). Specifically, alterations to the ECM using chondroitinase enzymatic digestion to deplete chondroitin sulfate proteoglycans in mature neurons preferentially reduce the density of inhibitory synapses (Dzyubenko et al., 2021). Thus, the significant decrease in the number of Gephyrin puncta observed in the distal dendrites following the expression of RNF13 DN may be indicative of an alteration to the ECM through a yet-to-be-established function of RNF13 (Fig. 6). As AP-3 has been shown to play a role in exocytosis (Ma et al., 2021), which greatly affects the ECM (Parihar et al., 2022), dileucine-altered variants may have influenced this pathway, given their loss of interaction with AP-3 (Cabana et al., 2021) and could explain the observed phenotype from the variants (Fig. 6). Overall, while RNF13's role in ECM regulation remains poorly understood, it would be an avenue to pursue for a better understanding of the underlying physiopathology of DEE73.

In a recent study, Taylor *et al.* conducted a comprehensive review of the literature and disease databases, identifying several additional variants, mainly caused by nonsense mutations, that manifest a DEE73-overlapping phenotype (Taylor et al., 2023). All the pathogenic or likely pathogenic variants are located between residues 292 and 312 (S292*, D293_S294ins*, Q300*, E301*, E307*, P310* and L311*), which leads to the hypothesis that a functional domain lies in this region (Taylor et al., 2023). Importantly, all the variants identified are heterozygous (Taylor et al., 2023). Autosomal dominant disorders are either a result of loss-of-function (LOF) caused by haploinsufficiency or by non-LOF mechanisms, which can be classified as dominant-negative (DN) or gain-of-function (GOF) effects (Gerasimavicius et al., 2022). It is unlikely that haploinsufficiency causes the disease associated with DEE73 (Taylor et al., 2023). In contrast, Edvardson *et al.* proposed that a GOF causes DEE73 (Edvardson et al., 2019). Specifically, they reported that XBP1 splicing and c-Jun phosphorylation levels are higher in fibroblasts and lymphoblasts derived from an affected individual carrying L311S after 48 h of tunicamycin treatment (Edvardson et al., 2019). As RNF13 was demonstrated to interact with IRE1α to promote ER stress-mediated apoptosis, Edvardson *et al.* proposed that the variants act as GOF proteins by enhancing this pathway (Edvardson et al., 2019). However, reducing autophagy levels increases IRE1α activity (Senft and Ronai, 2015), and RNF13 is increasingly recognized to regulate different types of autophagy (Miyakawa et al., 2022; Tan et al., 2022; Lin et al., 2023). The improper lysosomal location of L311S and L312P may alter autophagy, potentially leading to an increased IRE1α activity. While this hypothesis is highly speculative, it suggests that the evidence presented by Edvardson *et al.* is insufficient to confirm a GOF protein effect (Edvardson et al., 2019). Our findings show that L311S and L312P share characteristics comparable to those of the Ub ligase DN variant, indicating that impaired Ub ligase activity resulting from mislocalization of RNF13 might contribute to the mechanism underlying DEE73. Additionally, as supported by our experimental findings with the LL/AA variant, we propose that the functional domain associated with the DEE73-hotspot region is attributed to the residues 307–312 forming the dileucine motif. However, we cannot rule out the possibility of a GOF effect resulting from lysosomal degradation impairment and protein accumulation, particularly if the variants persist in a compartment for an extended period. While the exact cellular and molecular mechanisms remain to be clarified, this study provides valuable insights into how DEE73-associated genetic variants of RNF13 impact neuronal organization (Fig. 7).

5. Conclusion

Two missense mutations in the *RNF13* gene have been identified as the cause of the DEE73 disorder (Edvardson et al., 2019). Our previous study showed that these mutations alter a dileucine-based motif and ultimately disrupt the interaction with AP-3, resulting in a significantly reduced presence in lysosomes (Cabana et al., 2021). The current study builds on these findings, demonstrating that RNF13 L311S and L312P variants are trafficked toward their late endosomal location via an AP-1-dependent pathway in HeLa cells. Given the different functions of AP-1 and AP-3 in neurons, we report a significant increase in the presence of L311S and L312P in secondary and tertiary dendrites. Analysis reveals that alteration to the dileucine motif or the RING domain of RNF13 results in a redistribution of EEA1-positive early endosomes. Concurrently, the WT redistributes Lamp1-positive lysosomes in neurons. Furthermore, we observed that WT RNF13 protein increased the level of the anchoring protein PSD-95, while the variants blocked this effect. Notably, only the variants with altered dileucine motifs decreased the presence of Gephyrin in dendrites. Intriguingly, comparable results were obtained with the DN and the dileucine-motif altered variants, except for Gephyrin. These observations underscore the necessity for further investigation to elucidate the full scope of these phenomena. Firstly, transient expression provides a valuable opportunity to investigate the effect of variant proteins, but expression of RNF13 WT causes some phenotypes (van Dijk et al., 2014; Cabana et al., 2024). In this context, we established a baseline by selecting NT neurons as a control group. Even when variants exhibit no discernible difference with the NT, they may still exert a dominant negative effect on WT endogenous protein function if they do not manifest the same phenotype. Also, the reported effects might be directly caused by the genetic variants or result from a compensatory mechanism. While we reported multiple differences, further investigation through functional and electrophysiological

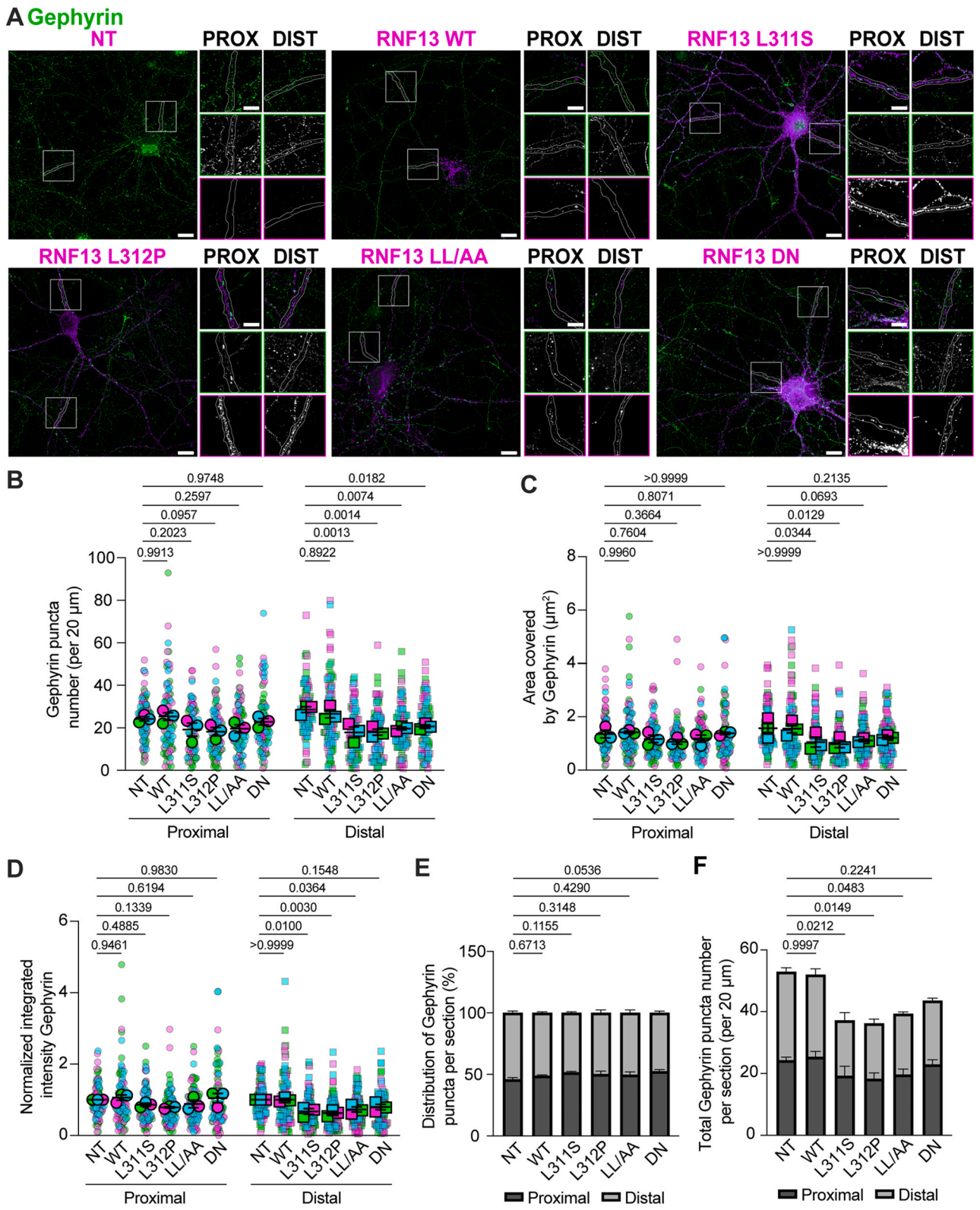

Fig. 6. Alterations to RNF13 dileucine motif decrease Gephyrin presence in dendrites. (A) Representative images of transfected primary cultures of hippocampal neurons show RNF13-HA (in purple) and the presence of endogenous inhibitory synapse marker Gephyrin (in green). Scale bars indicate 10 µm for the whole cell image and 5 µm for the boxed areas shown in higher magnification where the channels are presented as merged or separated (green boxes for Gephyrin, purple boxes for RNF13). PROX, proximal section, DIST, distal section. The jittered individual value plots represent the (B) number, (C) area covered, and (D) normalized signal intensity of Gephyrin in a 20 µm dendrites section taken directly after (proximal) or 50 µm away (distal) from the soma. Each colour represents an independent experiment, with smaller points representing the analysis of each dendrite segment (n = 90 dendrites) and larger points representing the mean of an independent experiment (N = 3). The summary bar plots represent the proportion of Gephyrin in the proximal and distal sections (E) and the total number of Gephyrin molecules in both sections (F). The data are expressed as mean ± SEM and analyzed using an RM two-way ANOVA with the Geisser-Greenhouse correction and Dunnett's multiple comparisons test with a single pooled variance. This was used to compare (B-E) simple effects within columns and (F) the mean row effect.

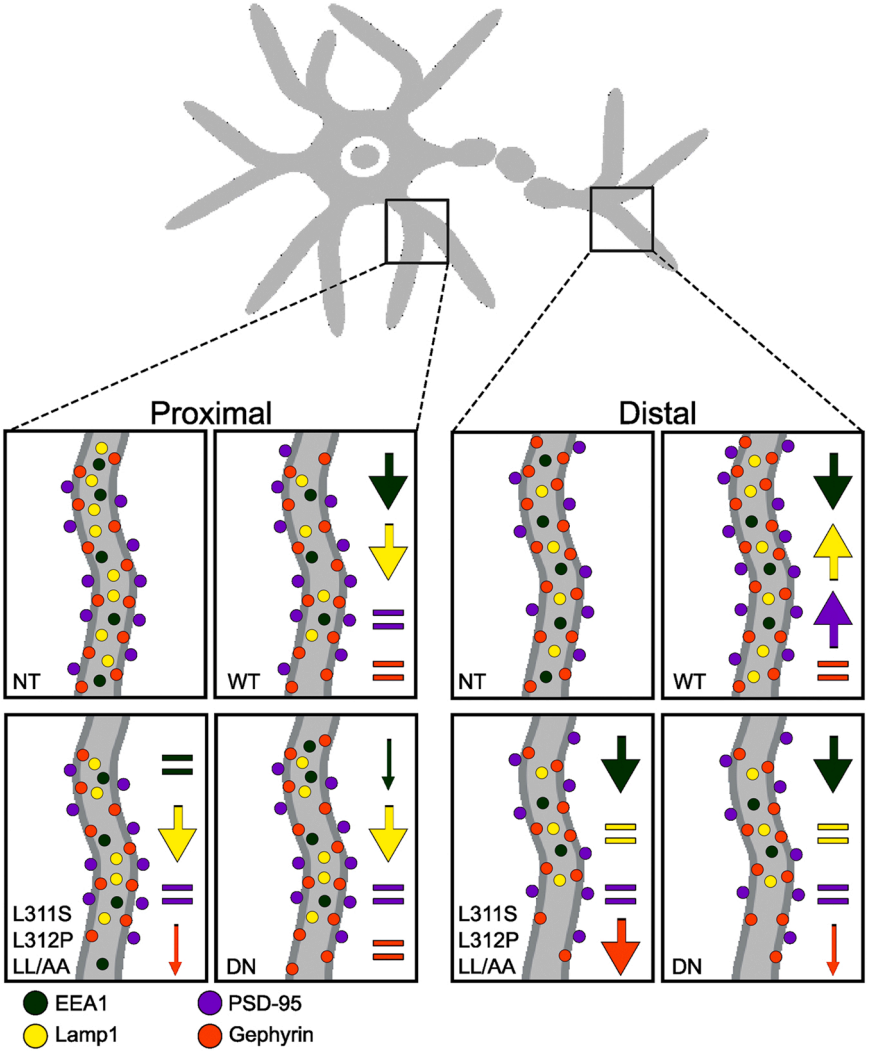

Fig. 7. Graphic summary of RNF13's impact on various dendritic components. This illustration summarizes the effects of RNF13 on the number of EEA1 (dark green), Lamp1 (yellow), PSD-95 (purple) and Gephyrin (orange) in proximal (left columns) or distal (right columns) dendrites of neurons. The columns represent neurons from control (NT) and RNF13, including wild-type (WT), dileucine-altered (L311S, L312P, LL/AA), and dominant-negative (DN) variants. For each condition, the larger arrows indicate significant changes compared to the NT group, while the smaller arrows denote minor and non-significant changes. The equal signs indicate no change in comparison to NT neurons.

experiments is necessary to establish the biologically relevant effects of these changes. Finally, future studies could use a double RNF13 mutant to provide valuable insights. This might confirm shared molecular pathways between the RING and the dileucine domains, affecting dendritic and synaptic determinants. Overall, this study provides the first insights into the impact of DEE73-associated genetic variants of RNF13 on neurons.

CRediT authorship contribution statement

Cabana Valérie C.: Writing – review & editing, Writing – original draft, Visualization, Validation, Resources, Methodology, Investigation, Formal analysis, Data curation, Conceptualization. **Lussier Marc P.:** Writing – review & editing, Writing – original draft, Visualization, Validation, Supervision, Resources, Project administration, Methodology, Funding acquisition, Formal analysis, Data curation, Conceptualization.

Conflicts of Interest

The authors declare that they have no known competing financial interests or personal relationships that could have appeared to influence the work reported in this paper.

Acknowledgements

This work was completed as part of the requirements for VCC's PhD thesis at the *Université du Québec à Montréal*. The authors thank Yann Aghiles Chabi for creating macros that allow automated image analysis and for commenting on the manuscript. The authors thank Jennifer Crawford for editing the manuscript. The *Centre d'Excellence en Recherche sur les Maladies Orphelines—Fondation Courtois* (CERMO-FC) funded part of this study via its program New Collaborative Research Initiatives and graduate scholarships awarded to V.C.C. (2020-2022). V.C.C was awarded a Ph.D. graduate scholarship from Le *Fonds de recherche du Québec – Nature et Technologies*. This work was partly supported by a Discovery Grant from the Natural Sciences and Engineering Research Council of Canada (RGPIN-2017-05392) and the American Epilepsy Society (Award ID 822781). Funding sources had no role in study design, data collection, analysis, or interpretation.

Appendix A. Supporting information

Supplementary data associated with this article can be found in the online version at doi:10.1016/j.ibneur.2025.04.004.

References

Arshad, M., Ye, Z., Gu, X., Wong, C.K., Liu, Y., Li, D., Zhou, L., Zhang, Y., Bay, W.P., Yu, V.C., Li, P., 2013. RNF13, a RING finger protein, mediates endoplasmic reticulum stress-induced apoptosis through the inositol-requiring enzyme (IRE1α)/c-Jun NH2-terminal kinase pathway. J. Biol. Chem. 288, 8726–8736.

Barnes, A.P., Polleux, F., 2009. Establishment of axon-dendrite polarity in developing neurons. Annu Rev. Neurosci. 32, 347–381.

Bocock, J.P., Carmicle, S., Chhotani, S., Ruffolo, M.R., Chu, H., Erickson, A.H., 2009. The PA-TM-RING protein RING finger protein13 is an endosomal integral membrane E3 ubiquitin ligase whose RING finger domain is released to the cytoplasm by proteolysis. FEBS J. 276, 1860–1877.

Cabana, V.C., Bouchard, A.Y., Sénécal, A.M., Ghilarducci, K., Kourrich, S., Cappadocia, L., Lussier, M.P., 2021. RNF13 dileucine motif variants L311S and L312P interfere with endosomal localization and AP-3 complex association. Cells 10.

Cabana, V.C., Lussier, M.P., 2022. From drosophila to human: biological function of E3 ligase godzilla and its role in disease. Cells 11.

Cabana, V.C., Sénécal, A.M., Bouchard, A.Y., Kourrich, S., Cappadocia, L., Lussier, M.P., 2024. AP-1 contributes to endosomal targeting of the ubiquitin ligase RNF13 via a secondary and novel non-canonical binding motif. J. Cell Sci. 137, jcs262035.

Cai, Q., Lu, L., Tian, J.-H., Zhu, Y.-B., Qiao, H., Sheng, Z.-H., 2010. Snapin-regulated late endosomal transport is critical for efficient autophagy-lysosomal function in neurons. Neuron 68, 73–86.

Chao, Y.-K., Chang, S.-Y., Grimm, C., 2023. Endo-Lysosomal Cation Channels and Infectious Diseases. In: Pedersen, S.H.F., Barber, D.L. (Eds.), In: Organelles in Disease. Springer International Publishing, Cham, pp. 259–276.

Cheng, H., Wang, A., Meng, J., Zhang, Y., Zhu, D., 2015. Enhanced metastasis in RNF13 knockout mice is mediated by a reduction in GM-CSF levels. Protein Cell 6, 746–756.

Choii, G., Ko, J., 2015. Gephyrin: a central GABAergic synapse organizer. Exp. Mol. Med. 47 e158-e158.

Dell'Angelica, E.C., Bonifacino, J.S., 2019. Coatopathies: genetic disorders of protein coats. Annu Rev. Cell Dev. Biol. 35, 131–168.

van Dijk, J.R., Yamazaki, Y., Palmer, R.H., 2014. Tumour-associated mutations of PA-TM-RING ubiquitin ligases RNF167/RNF13 identify the PA domain as a determinant for endosomal localization. Biochem. J. 459, 27–36.

Donato, A., Kagias, K., Zhang, Y., Hilliard, M.A., 2019. Neuronal sub-compartmentalization: a strategy to optimize neuronal function. Biol. Rev. Camb. Philos. Soc. 94, 1023–1037.

Dzyubenko, E., Fleischer, M., Manrique-Castano, D., Borbor, M., Kleinschnitz, C., Faissner, A., Hermann, D.M., 2021. Inhibitory control in neuronal networks relies on the extracellular matrix integrity. Cell. Mol. Life Sci. 78, 5647–5663.

Edvardson, S., Nicolae, C.M., Noh, G.J., Burton, J.E., Punzi, G., Shaag, A., Bischetsrieder, J., De Grassi, A., Pierri, C.L., Elpeleg, O., Moldovan, G.L., 2019. Heterozygous RNF13 gain-of-function variants are associated with congenital microcephaly, epileptic encephalopathy, blindness, and failure to thrive. Am. J. Hum. Genet. 104, 179–185.

Gerasimavicius, L., Livesey, B.J., Marsh, J.A., 2022. Loss-of-function, gain-of-function and dominant-negative mutations have profoundly different effects on protein structure. Nat. Commun. 13, 3895.

Gerrow, K., Romorini, S., Nabi, S.M., Colicos, M.A., Sala, C., El-Husseini, A., 2006. A preformed complex of postsynaptic proteins is involved in excitatory synapse development. Neuron 49, 547–562.

Goo, M.S., Sancho, L., Slepak, N., Boassa, D., Deerinck, T.J., Ellisman, M.H., Bloodgood, B.L., Patrick, G.N., 2017. Activity-dependent trafficking of lysosomes in dendrites and dendritic spines. J. Cell Biol. 216, 2499–2513.

Grochowska, K.M., Andres-Alonso, M., Karpova, A., Kreutz, M.R., 2022. The needs of a synapse—How local organelles serve synaptic proteostasis. EMBO J. 41, e110057.

Guardia, C.M., De Pace, R., Mattera, R., Bonifacino, J.S., 2018. Neuronal functions of adaptor complexes involved in protein sorting. Curr. Opin. Neurobiol. 51, 103–110.

Guerrini, R., Conti, V., Mantegazza, M., Balestrini, S., Galanopoulou, A.S., Benfenati, F., 2023. Developmental and epileptic encephalopathies: from genetic heterogeneity to phenotypic continuum. Physiol. Rev. 103, 433–513.

Guo, X., Mattera, R., Ren, X., Chen, Y., Retamal, C., González, A., Bonifacino, J.S., 2013. The adaptor protein-1 μ1B subunit expands the repertoire of basolateral sorting signal recognition in epithelial cells. Dev. Cell 27, 353–366.

Hu, Y.B., Dammer, E.B., Ren, R.J., Wang, G., 2015. The endosomal-lysosomal system: from acidification and cargo sorting to neurodegeneration. Transl. Neurodegener. 4, 18.

Huotari, J., Helenius, A., 2011. Endosome maturation. Embo J. 30, 3481–3500.

Li, P., Merrill, S.A., Jorgensen, E.M., Shen, K., 2016. Two clathrin adaptor protein complexes instruct axon-dendrite polarity. Neuron 90, 564–580.

Lin, Z., Yang, P., Hu, Y., Xu, H., Duan, J., He, F., Dou, K., Wang, L., 2023. RING finger protein 13 protects against nonalcoholic steatohepatitis by targeting STING-relayed signaling pathways. Nat. Commun. 14, 6635.

Liu, W., Wang, Y., Liu, S., Zhang, X., Cao, X., Jiang, M., 2024. E3 ubiquitin ligase RNF13 suppresses TLR lysosomal degradation by promoting LAMP-1 proteasomal degradation. Adv. Sci., e2309560

Lussier, M.P., Cayouette, S., Lepage, P.K., Bernier, C.L., Francoeur, N., St-Hilaire, M., Pinard, M., Boulay, G., 2005. MxA, a member of the dynamin superfamily, interacts with the ankyrin-like repeat domain of TRPC. J. Biol. Chem. 280, 19393–19400.

Lussier, M.P., Herring, B.E., Nasu-Nishimura, Y., Neutzner, A., Karbowski, M., Youle, R. J., Nicoll, R.A., Roche, K.W., 2012. Ubiquitin ligase RNF167 regulates AMPA receptor-mediated synaptic transmission. Proc. Natl. Acad. Sci. 109, 19426–19431.

Ma, Z., Islam, M.N., Xu, T., Song, E., 2021. AP-3 adaptor complex-mediated vesicle trafficking. Biophys. Rep. 7, 91–100.

Miyakawa, K., Nishi, M., Ogawa, M., Matsunaga, S., Sugiyama, M., Nishitsuji, H., Kimura, H., Ohnishi, M., Watashi, K., Shimotohno, K., Wakita, T., Ryo, A., 2022. Galectin-9 restricts hepatitis B virus replication via p62/SQSTM1-mediated selective autophagy of viral core proteins. Nat. Commun. 13, 531.

Navarro Negredo, P., Edgar, J.R., Wrobel, A.G., Zaccai, N.R., Antrobus, R., Owen, D.J., Robinson, M.S., 2017. Contribution of the clathrin adaptor AP-1 subunit μ1 to acidic cluster protein sorting. J. Cell Biol. 216, 2927–2943.

Nelson, A.D., Bender, K.J., 2021. Dendritic integration dysfunction in neurodevelopmental disorders. Dev. Neurosci. 43, 201–221.

Nishiyama, J., 2019. Plasticity of dendritic spines: molecular function and dysfunction in neurodevelopmental disorders. Psychiatry Clin. Neurosci. 73, 541–550.

Parihar, K., Nukpezah, J., Iwamoto, D.V., Janmey, P.A., Radhakrishnan, R., 2022. Data driven and biophysical insights into the regulation of trafficking vesicles by extracellular matrix stiffness. iScience 25, 104721.

Park, S.Y., Guo, X., 2014. Adaptor protein complexes and intracellular transport. Biosci. Rep. 34.

Penzes, P., Cahill, M.E., Jones, K.A., VanLeeuwen, J.-E., Woolfrey, K.M., 2011. Dendritic spine pathology in neuropsychiatric disorders. Nat. Neurosci. 14, 285–293.

Platzer, K., Sticht, H., Bupp, C., Ganapathi, M., Pereira, E.M., Le Guyader, G., Bilan, F., Henderson, L.B., Lemke, J.R., Taschenberger, H., Brose, N., Abou Jamra, R., Wojcik, S.M., 2022. De novo missense variants in cause a developmental and epileptic encephalopathy due to impaired gabaergic neurotransmission. Ann. Neurol. 92, 958–973.

Rebiai, R., Givogri, M.I., Gowrishankar, S., Cologna, S.M., Alford, S.T., Bongarzone, E.R., 2021. Synaptic function and dysfunction in lysosomal storage diseases. Front. Cell. Neurosci. 15.

Roney, J.C., Cheng, X.T., Sheng, Z.H., 2022. Neuronal endolysosomal transport and lysosomal functionality in maintaining axonostasis. J. Cell Biol. 221.

Saito, S., Honma, K., Kita-Matsuo, H., Ochiya, T., Kato, K., 2005. Gene expression profiling of cerebellar development with high-throughput functional analysis. Physiol. Genom. 22, 8–13.

Sanger, A., Hirst, J., Davies, A.K., Robinson, M.S., 2019. Adaptor protein complexes and disease at a glance. J. Cell Sci. 132, jcs222992.

Senft, D., Ronai, Z.A., 2015. UPR, autophagy, and mitochondria crosstalk underlies the ER stress response. Trends Biochem. Sci. 40, 141–148.

Tan, H.W.S., Lu, G., Dong, H., Cho, Y.-L., Natalia, A., Wang, L., Chan, C., Kappei, D., Taneja, R., Ling, S.-C., Shao, H., Tsai, S.-Y., Ding, W.-X., Shen, H.-M., 2022. A degradative to secretory autophagy switch mediates mitochondria clearance in the absence of the mATG8-conjugation machinery. Nat. Commun. 13, 3720.

Tang, T., Yang, Z.-y, Wang, D., Yang, X.-y, Wang, J., Li, L., Wen, Q., Gao, L., Bian, X.-w, Yu, S.-c, 2020. The role of lysosomes in cancer development and progression. Cell Biosci. 10, 131.

Taylor, A., Kashyape, P.S., Jain, R., El Naofal, M., Tayoun, A.A., 2023. Heterozygous gain of function variants in a critical region of RNF13 cause congenital microcephaly, epileptic encephalopathy, blindness, and failure to thrive. Am. J. Med. Genet. A 191, 2723–2727.

Tranque, P., Crossin, K.L., Cirelli, C., Edelman, G.M., Mauro, V.P., 1996. Identification and characterization of a RING zinc finger gene (C-RZF) expressed in chicken embryo cells. Proc. Natl. Acad. Sci. 93, 3105–3109.

Winckler, B., Faundez, V., Maday, S., Cai, Q., Guimas Almeida, C., Zhang, H., 2018. The Endolysosomal system and proteostasis: from development to degeneration. J. Neurosci. 38, 9364–9374.

Yap, C.C., Digilio, L., McMahon, L.P., Wang, T., Winckler, B., 2022. Dynein is required for Rab7-dependent endosome maturation, retrograde dendritic transport, and degradation. J. Neurosci. 42, 4415.

Yap, C.C., Winckler, B., 2022. Spatial regulation of endosomes in growing dendrites. Dev. Biol. 486, 5–14.

Yoo, K.-S., Lee, K., Oh, J.-Y., Lee, H., Park, H., Park, Y.S., Kim, H.K., 2019. Postsynaptic density protein 95 (PSD-95) is transported by KIF5 to dendritic regions. Mol. Brain 12, 97.

Zhang, J., Cheng, Y., Xing, Q., 2024. Adaptor proteins in neuronal development and neurological disorders: a comprehensive review of their roles and importance. J. Bio-X Res. 7, 0003.

Zhang, Q., Li, Y., Zhang, L., Yang, N., Meng, J., Zuo, P., Zhang, Y., Chen, J., Wang, L., Gao, X., Zhu, D., 2013. E3 ubiquitin ligase RNF13 involves spatial learning and assembly of the SNARE complex. Cell Mol. Life Sci. 70, 153–165.

Zhang, Q., Meng, Y., Zhang, L., Chen, J., Zhu, D., 2009. RNF13: a novel RING-type ubiquitin ligase over-expressed in pancreatic cancer. Cell Res. 19, 348–357.